Direct observation of hydrodynamic instabilities in a driven non-uniform colloidal dispersion†

Adam Wysocki,*[a] C. Patrick Royall,*[b] Roland G. Winkler,[c] Gerhard Gompper,[c] Hajime Tanaka,[d] Alfons van Blaaderen[e] and Hartmut Löwen[a]

Received 27th November 2008, Accepted 3rd February 2009
First published as an Advance Article on the web 20th February 2009
DOI: 10.1039/b821250c

A Rayleigh–Taylor-like instability of a dense colloidal layer under gravity in a capillary of microfluidic dimensions is considered. We access all relevant lengthscales with particle-level microscopy and computer simulations which incorporate long-range hydrodynamic interactions between the particles. By tuning the gravitational driving force, we reveal a mechanism whose growth is connected to the fluctuations of specific wavelengths, non-linear pattern formation and subsequent diffusion-dominated relaxation. Our linear stability theory captures the initial regime and thus predicts mixing conditions, with important implications for fields ranging from biology to nanotechnology.

Particulate dispersions have long been subjected to external fields as a means to separate different constituents; in particular, sedimentation is important not only for analytical but also for preparative purposes.[1] For bulk systems, successful separation depends crucially upon avoiding hydrodynamic instabilities. The development of microfluidics[2] has made it possible to exploit the suppression of turbulence at small lengthscales in order to design novel separation devices;[3] on the other hand, this significantly increased stability against mechanical perturbations severely limits mixing, which is needed for many ‘lab-on-a-chip’ applications. Often strong external fields[4] or complex fabrication[5] are required to produce the hydrodynamic instabilities required for efficient mixing.

Experiments[6,7] and computer simulations[8] which study velocity fluctuations have played a crucial role in our understanding of how dispersions respond to external driving fields, in particular to gravity. The motion of a solute particle is characterised by a Peclet number $Pe = \tau_D/\tau_S$, which is the ratio between the time it takes a particle to diffuse its own radius $\tau_D = \sigma^2/(4D)$, where σ is the diameter and D is the diffusion constant, and the time it takes to sediment the same distance $\tau_S = \sigma/(2V_S)$, where V_S is the sedimentation velocity. A Peclet number of order unity is the dividing line between colloidal ($Pe \leq 1$) and granular systems ($Pe \gg 1$), *i.e.* Pe measures the importance of Brownian motion. Most attempts at a quantitative description of sedimentation to date considered a homogenously distributed dispersion as the initial state. For preparative purposes, on the other hand, starting with a particle-rich layer on top of pure solvent is more relevant as it enables the separation of particles depending on their sedimentation coefficient. However, this configuration is unstable with respect to gravity. The particle velocities become correlated, which leads to emergent density fluctuations and consequently more rapid sedimentation than Stokes’ flow alone. It is well known that many practical particle concentrations develop this Rayleigh–Taylor (RT) like instability. This provides an avenue by which the system may be successfully mixed on the one hand, conversely, this very mixing leads, chaotically, to a scenario in which separation does not occur. For stable separation, it is essential to avoid the RT instability. It is possible to use a density gradient to counteract the instabilities.[1]

The ‘original’ Rayleigh–Taylor instability, which occurs if a heavy, immiscible fluid layer is placed on top of a lighter one has been intensively studied for the case of a simple Newtonian fluid both by theory,[9] simulation[10] and experiment, and is observed in granular matter,[11–13] in surface tension dominated colloid-polymer mixtures[14] and in a suspension of dielectric particles exposed to an ac electric field gradient,[15] but a particle-resolved measurement and simulation is missing for colloidal suspensions.

Here we consider a suspension of colloidal hard spheres (without surface tension) of microfluidic dimensions, in which we have access to all relevant length scales, from the single-particle level to the full system. A systematic study of sedimentation in an *inhomogenous* system is presented. We employ three approaches: experiment, computer simulation and theory. The experimental realisation is provided by confocal microscopy at the single-particle level,[16] while the simulation is a particle-based mesoscale technique[17] which

---

[a] *Institut für Theoretische Physik II, Heinrich-Heine-Universität Düsseldorf, Universitätsstrasse 1, D-40225 Düsseldorf, Germany. E-mail: adam@thphy.uni-duesseldorf.de*
[b] *School of Chemistry, University of Bristol, Bristol, UK BS8 1TS. E-mail: paddy.royall@bristol.ac.uk*
[c] *Institut für Festkörperforschung, Forschungszentrum Jülich, D-52425 Jülich, Germany*
[d] *Institute of Industrial Science, University of Tokyo, 4-6-1 Komaba, Meguro-ku, Tokyo 153-8505, Japan*
[e] *Soft Condensed Matter Group, Debye Institute for Nanomaterials Science, Utrecht University, PO Box 80000, 3508 TA Utrecht, The Netherlands*

† Electronic supplementary information (ESI) available: Movie 1: simulation: side view of the simulation box which contains $N = 33\,858$ colloidal particles and $N_s = 32\,118\,397$ solvent particles (not displayed). The dimensions of the simulation box are $L/\sigma = 18$ and $L_y/\sigma = L_z/\sigma = 81$. The value of the Peclet number is $Pe = 1.6$. The duration of the movie is $\approx 22\ \tau_S$ and the time between two frames is $\approx 0.04\ \tau_S$. The thickness of the slice is 2σ.
Movie 2: simulation: top view of the simulation box for the same parameters as in Video 1. The height of the slice of thickness 1.5σ is $x/L=2/3$.
Movie 3: experiment: side view of the 50 μm capillary ($L/\sigma=18$) for the Peclet number $Pe = 1.1$. The resolution is 91×256 pixels with a pixel size of 0.893 μm. The duration of the movie is 640 s $\approx 24\tau_S$ and the time between two frames is 10 s $\approx 0.37\tau_S$.
Movie 4: experiment: top view of the 50 μm capillary for the same parameters as in Video 3. The resolution is 256×256 pixels and the height of the slice is $x/L=2/3$.
Movie 5: experiment: side view of the 100 μm capillary ($L/\sigma = 36$) for the Peclet number $Pe = 2.42$. The resolution is 180×256 pixels with a pixel size of 0.893 μm. The duration of the movie is 640 s $\approx 53\tau_S$ and the time between two frames is 10 s $\approx 0.83\tau_S$. See DOI: 10.1039/b821250c

captures the direct interactions between the colloidal particles, and, crucially, the solvent which mediates the hydrodynamic interactions and whose backflow drives the RT instability. Our results at short times are modelled with a linear stability analysis.[9]

The RT instability is thought of as a fluctuation in the interface between two fluids. Since in a hard-sphere suspension there is no phase separation, we consider a continuous density profile, albeit rapidly varying. To capture the lateral fluctuations, we consider the stability of this density and associated pressure profile against fluctuations of wavelength λ in a horizontal plane perpendicular to gravity. We consider a slit geometry of height L which is sketched in Fig. 1a. In the absence of surface tension, the fluctuations of all wavelengths are in principle unstable, but short wavelength fluctuations are washed out by diffusion of the colloidal particles and so do not grow exponentially.[18,19]

Our linear stability analysis, which reveals the stable and fast-growing wavelengths of fluctuations, is based on a continuum hydrodynamics approach where the colloidal dispersion is considered as an incompressible one-component fluid with inhomogeneous mass density $\rho(x)$ and corresponding kinematic viscosity $\nu(x)$ as obtained from the Saito representation.[20] The spatially varying density profile is given by $\rho(x) = \phi(x)\rho_c + (1 - \phi(x))\rho_s$, where ρ_c and ρ_s are the mass densities of the colloidal particles and the solvent. The colloidal packing fraction profile $\phi(x)$ is an input from an equilibrated simulation for inverted gravity. The stability of the initial density $\rho(x)$ and pressure $p(x)$ profiles against pertubations $\delta\rho \propto \delta p \propto \exp(i(k_y y + k_z z) + n(k)t)$ with wave number $k = (k_y^2 + k_z^2)^{1/2}$ in the yz plane and the growth rate n is calculated *via* the linearized Navier–Stokes equations[9] resulting in the eigenvalue problem

$$n\left\{(\rho u_x')' - \rho k^2 u_x\right\} = \left\{\nu(u_x''' - k^2 u_x') + \nu'(u_x'' + k^2 u_x)\right\}' - k^2\left\{\frac{g}{n}\rho' u_x + 2\nu' u_x' + \nu\left(u_x'' - k^2 u_x\right)\right\} \tag{1}$$

with the spatial derivative $\ldots' = d\ldots/dx$, the strength of the gravitational field g and the fluid velocity field in the direction of gravity $u_x(x)$. For a system confined between two rigid walls we impose $u_x = 0$ along with the no-slip boundary conditions $du_x/dx = 0$ at $x = 0, L$. We account for colloid diffusion by the correction term $n^*(k) = n(k) - Dk^2$,[18,19] with diffusion constant $D = k_B T/(3\pi\eta_s\sigma)$, colloid diameter σ and dynamic solvent viscosity η_s.

In our computer simulation, which includes solvent-mediated momentum transfer between the colloidal particles, we consider a suspension of $N = 15\,048$ hard sphere particles of mass M immersed in a bath of typically $N_s = 14,274\,843$ solvent particles of mass m and number density $n_s = N_s/V$. The solvent particles are subjected to multi-particle collision dynamics,[17,21] which consists of two steps. In the streaming step, solvent particles move ballistically for a time δt. In the collision step, particles are sorted into cubic cells of size a, and their velocities relative to the centre-of-mass velocity of each cell are rotated by an angle α around a random axis. We employed the parameters $\delta t = 0.2\sqrt{ma^2/(k_B T)}$, $\alpha = 3\pi/4$, $n_s a^3 = 5$ and $M = 167m$ in order to achieve the hierarchy of time scales and the same hydrodynamic numbers as in the experiment, see ref. 8,22 for details. To enforce the no-slip boundary condition on the colloid surface and the confining walls a stochastic-reflection method[23] is

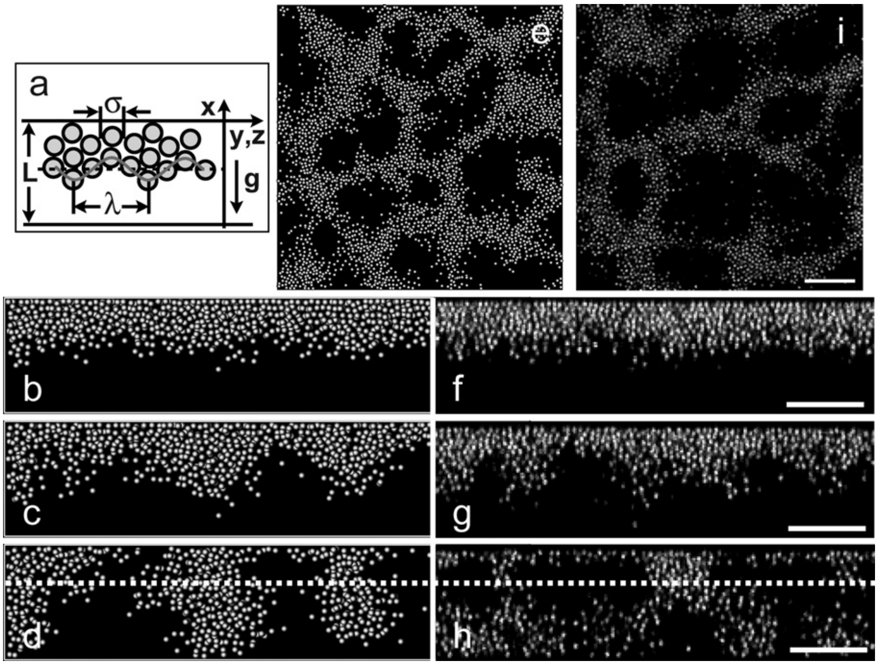

Fig. 1 (a) A schematic illustrating the spatial parameters σ, λ and L. (b–e) Simulation snapshots of a system which contains $N = 33\,858$ colloidal particles and $N_s = 32\,118\,397$ solvent particles (not displayed) in a simulation box with dimensions $L/\sigma = 18$ and $L_y/\sigma = L_z/\sigma = 81$. The value of the Peclet number is $Pe = 1.6$. (b–d) Time series of the system at time $t/\tau_S = 3.2$ (b), 6.4 (c), 9.6 (d). The snapshots are slices of thickness 2σ done in the xy plane. (e) Slice of thickness 2σ in the yz plane at time $t/\tau_S = 9.6$. The height of the yz plane is $x/L = 2/3$, as indicated by the dashed line in (d). (f–i) Experimental realisation of the Rayleigh–Taylor-like instability. (f–h) Time series of images taken with a confocal microscope in the xy plane for the parameters $\phi = 0.15$, $Pe = 1.1$ and $L/\sigma = 18$ at times $t/\tau_S = 1.43$ (f), 5.5 (g), 11.22 (h). (i) Slice in the yz plane at a height $x/L = 2/3$ (indicated by the dashed line in (h)) at time $t/\tau_S = 11.22$. In (f–i) the scale bars denote 40 μm. (f–h) are 2D images reconstructed from 3D confocal scans.

applied. Statistical averages for time-dependent quantities are performed over 200 independent configurations.

In our single-particle level confocal microscopy experiments we used polymethylmethacrylate colloids sterically stabilised with polyhydroxy-stearic acid. The colloids were labeled with the fluorescent dye coumarine and had a diameter $\sigma = 2.8$ μm with around 4% polydispersity as determined by static light scattering. To almost match the colloid refractive index we used a solvent mixture of cis-decalin and cyclohexyl bromide (CHB), which we tuned to yield different Peclet numbers, owing to changes in the degree of density mismatch between the colloids and the solvent. Specifically, $Pe = 1.1$ and $Pe = 2.4$ correspond to 80% and 87.5% CHB by weight respectively. Since $Pe = \sigma/(2l_g)$ where l_g is the gravitational length, we independently determine the Peclet number by measuring the gravitational length of the system in the sedimentation-diffusion equilibrium, following ref. 24. We measured the dynamic viscosity of the solvents with a rheometer and obtained $\eta_s \approx 2.3$ mPa s. The room temperature during the experiments was fixed at 25 °C. The characteristic time to diffuse a radius $\tau_D = \sigma^2/(4D) \approx 29$ s. The data were collected on a Leica SP5 confocal microscope, fitted with a resonant scanner, at a typical scan-time of around 10 s per 3D data set. While this scan-time is comparable to the time to diffuse a radius, we note that the time to scan a particle diameter is less than a second, during which time the particle has little chance to move: thus we are able to capture the local structure at the particle level, while for greater lengthscales, although some local rearrangement may occur, the larger structure diffuses little on the timescale of 10 s. Prior equilibration was achieved by placing the suspension overnight such that it sedimented across a thin (typically 50 μm) capillary. The capillary was then inverted, and the evolution under sedimentation was followed.

We begin our discussion by presenting snapshots of the system, in Fig. 1b–e from computer simulation, and in Fig. 1f–i from confocal microscopy. The similarity is remarkable, and we note that, at the very least, our simulation qualitatively reproduces the experiment.

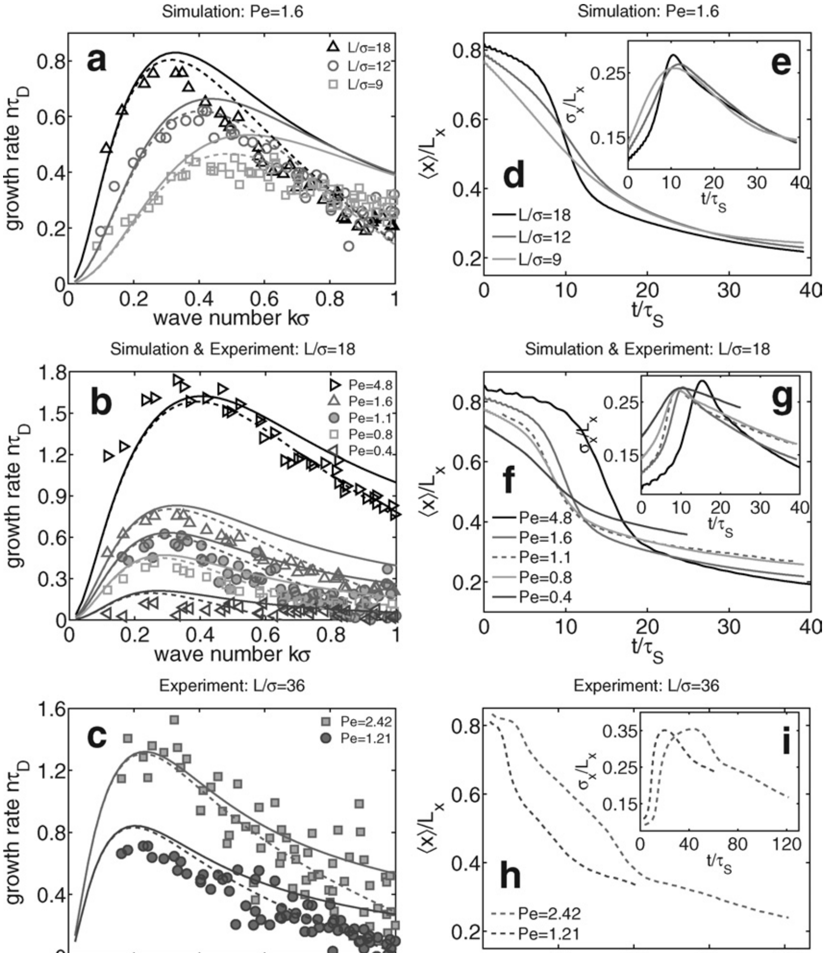

Fig. 2 (a–c) Growth rate $n\tau_D$ *versus* wave number $k\sigma = 2\pi\sigma/\lambda$. (a) Simulation results of $n(k)$ for different wall separation distances $L/\sigma = 18$, 12, 9 and fixed $Pe = 1.6$. (b) Simulation and experimental results of $n(k)$ for different Peclet numbers $Pe = 4.8$, 1.6, 1.1, 0.8, 0.4 and fixed $L/\sigma = 18$. (c) Experimental results of $n(k)$ for different Peclet numbers $Pe = 2.42$, 1.21 and fixed $L/\sigma = 36$. The open symbols are the results obtained from simulation, filled symbols are experimental results, solid lines represent the solutions from the instability analysis and the dashed lines are the same numerical solutions plus the diffusion correction. First moment of the colloid density $\langle x\rangle/L$ (d), (f), (h) and second moment of the colloid density σ_x/L (e), (g), (i) *versus* time t/τ_S. Solid lines indicate simulation data whereas the dashed lines indicate experimental data. (d and e) $L/\sigma = 18$, 12, 9 and $Pe = 1.6$. (f and g) $Pe = 4.8$, 1.6, 1.1, 0.8, 0.4 and $L/\sigma = 18$. (h and i) $Pe = 2.42$, 1.21 and $L/\sigma = 36$.

For a quantitative comparison, we consider the dispersion relation of wave number against growth rate in Fig. 2b. The time evolution in the development of the RT instability with a characteristic wavelength is clear. While snapshots in the gravity plane (Fig. 1b, c, d, f, g, and h) illustrate the overall process of sedimentation, snapshots in the horizontal *yz* plane show the transient pattern or network-like structure that results from the RT instability (Fig. 1e and i). At later times, the network structure decays and a laterally homogenous density profile develops where the colloids start to form a layer at the bottom of the cell which becomes more compact with time. The time evolution is shown in detail in Movies 1–4.†

The linear stability analysis predicts the existence of the initially fastest growing wavelengths in the RT instability. We plot the results of the linear stability analysis for a range of slit widths L keeping Pe fixed, and for a variety of Peclet numbers keeping L fixed in Fig. 2a, b and c respectively. The dimensionless growth rates, $n\tau_D$, are plotted as a function of wave number $k\sigma = 2\pi\sigma/\lambda$, where λ is the wavelength of the fluctuations as indicated in Fig. 1a. Without diffusion, fluctuations at all wave numbers are unstable, as shown by the solid lines in Fig. 2a, b and c. Due to diffusion, we find that growth rates at higher wavevectors are suppressed as expected, *i.e.*, diffusion destroys the Rayleigh–Taylor instability at sufficiently small wavelengths. We find excellent agreement between the theory with diffusion and both simulation and experimental data, up to $k\sigma \approx 1$, which is surprising for a coarse-grained continuum description. With decreasing wall separation L, the growth rate n_{max} decreases and k_{max} increases, see Fig. 2a. Since the fluid velocity in the gravity direction decreases as e^{-kx}, where x is the distance from the interface, only long wavelength undulations feel the presence of the walls.[9,25] Fig. 2b and c show that for fixed L, driving the sedimentation more strongly by increasing the Peclet number leads to an increase in the wave number of the fastest growing undulation k_{max}, and the corresponding growth rate n_{max}. So far we have considered only the linear regime of the instability, which is valid at small times, when the amplitude of the fluctuations is smaller than the wavelength. Our experiments and simulations permit detailed access to all relevant time- and length scales in the non-linear regime, where the colloids form foam-like structures in the (confined) *xz* plane (Fig. 1c and g) and a network-like structure in the *yz* plane (Fig. 1e and i) appears. Apparently, both continue to exhibit the characteristic length scale $\lambda_{max} = 2\pi/k_{max}$ of the fastest growing wavelength in the linear regime. In order to quantify the different regimes of the instability we use the first moment of the density $\langle x \rangle$, *i.e.* the centre of mass of the colloid coordinates and the second moment of the density $\sigma_x^2 = \langle x^2 \rangle - \langle x \rangle^2$. Here, $\langle x \rangle$ is a measure of the degree of sedimentation, while σ_x quantifies the extent to which the instability spreads out the colloids in the gravity direction. Three regimes are clearly visible in Fig. 2d, f, h, e, g and i. Firstly we find the linear regime in which the flat interface develops undulations and hence $\langle x \rangle$ slowly decreases and σ_x slowly increases, secondly the non-linear regime where 'droplets' of colloid-rich material fall to the bottom and therefore $\langle x \rangle$ sharply decreases and σ_x sharply increases, and thirdly the regime in which the colloids start to form a layer at the bottom of the cell which becomes more compact with time under settling as can be seen from the slow decrease of both $\langle x \rangle$ and σ_x. Clear agreement between simulation and experimental data can be seen from Fig. 2f and g.

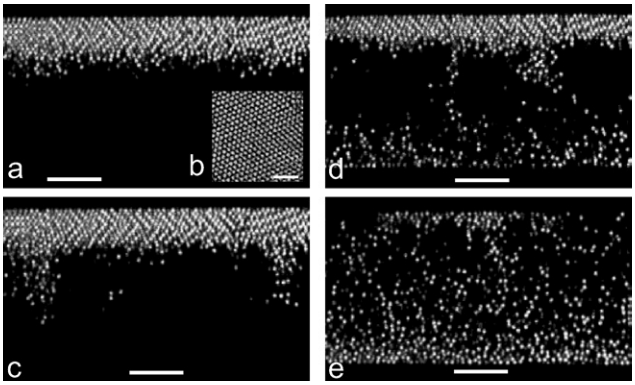

Fig. 3 Time series of images taken with a confocal microscope in the *xy* plane for the parameters $\phi = 0.15$, $Pe = 2.42$ and $L/\sigma = 36$ at times $t/\tau_S =$ 3.1 (a), 8.1 (c), 24.6 (d) and 56 (e). The crystalline layers are clearly visible. (b) is a slice in the *yz* plane approximately in the middle of the colloidal crystal in (a). The secondary instability occurs at $t/\tau_S \approx$ 20–30, see (d). In (a, c–e) the scale bar denotes 40 μm and 20 μm in (b).

In the case of a rather large slit width $L/\sigma = 36$, there is a sufficiently high sediment for a region of colloidal crystal to form, see Fig 3 and Movie 5.† Since the crystal has a finite (albeit small) yield stress, the only flow we observe initially occurs in a thin fluid layer between the crystal and the lower solvent region *via* narrow vertical tubes, in marked contrast to Fig. 1 b–d. The crystal melts layer by layer until finally it becomes sufficiently thin that it peels off the wall in a second instability, which leads to a change of slope for the $Pe = 2.42$ line in Fig. 2h and i at $t/\tau_S \approx$ 20–30, see Fig. 3 d, until most of the particles have sedimented down (Fig. 3 e). This observation of driven surface melting at the single-particle level has the potential to provide new insight into this poorly understood phase transition under non-equilibrium conditions.

Using simulation and experimental techniques, we have presented a quantitative analysis of a hydrodynamic instability in a colloidal system at a microfluidic lengthscale. Our results show excellent agreement between experiment and simulation, showing that the latter accurately describes the fundamentally and practically important phenomena caused by hydrodynamic instabilities. Furthermore, by employing a simple theoretical treatment to the initial linear behaviour, we find considerable predictive power. The theory can flexibly be used to predict conditions for separation and mixing. We also note that the theory reveals even the length scale of the network structure that results from the instability. We finally emphasise that the full access and accuracy to all relevant length scales in this problem allowed for the observation of novel phenomena, not yet explored further, such as the inverse gravity induced crystal melting. Finally, it would be interesting to explore the instability for various initial colloidal density profiles (as *e.g.* sharp-kink-like profiles, linear density gradients or softened profiles originating from wall charges) and for different colloidal interactions as relevant for charged particles.[26]

Acknowledgements

We acknowledge ZIM for computing time. A. W. thanks E. W. Laedke and G. Lehmann for help. We acknowledge A. A. Louis and J. T. Padding for discussions. The authors are grateful to Didi Derks for a kind gift of PMMA colloids. A. W., R. G. W., G. G., H. L. and A. v. B. thank the DFG/FOM for support in particular *via* SFB TR6 (projects A3, A4 and D3). C. P. R. acknowledges the Royal Society for Funding. H. T. acknowledges a grant-in-aid from MEXT.

Notes and references

1 V. N. Manoharan, M. T. Elsesser and D. J. Pine, *Science*, 2003, **301**(5632), 483–487.

2 T. M. Squires and S. R. Quake, *Rev. Mod. Phys.*, 2005, **77**(3), 977.

3 D. Huh, J. Bahng, Y. Ling, H.-H. Wei, O. Kripfgans, J. Fowlkes, J. Grotberg and S. Takayama, *Anal. Chem.*, 2007, **79**(4), 1369–1376.

4 A. O. El Moctar, N. Aubry and J. Batton, *Lab on a Chip*, 2003, **3**(4), 273–280.

5 C. Simonnet and A. Groismann, *Phys. Rev. Lett.*, 2005, **94**, 134501.

6 P. N. Segre, H. E. and P. Chaikin, *Phys. Rev. Lett.*, 1997, **79**, 2574–2577.

7 C. P. Royall, J. Dzubiella, M. Schmidt and A. van Blaaderen, *Phys. Rev. Lett.*, 2007, **98**(18), 188304.

8 J. T. Padding and A. A. Louis, *Phys. Rev. E*, 2008, **77**(1), 011402.

9 S. Chandrasekhar, *Hydrodynamic and Hydromagnetic Stability*, Oxford University Press, Oxford, 1961.

10 K. Kadau, T. C. Germann, N. G. Hadjiconstantinou, P. S. Lomdahl, G. Dimonte, B. L. Holian and B. J. Alder, *Proc. Natl. Acad. Sci. USA*, 2004, **101**(16), 5851–5855.

11 C. Völtz, W. Pesch and I. Rehberg, *Phys. Rev. E*, 2001, **65**(1), 011404.

12 J. L. Vinningland, Ø. Johnsen, E. G. Flekkøy, R. Toussaint and K. J. Måløy, *Phys. Rev. Lett.*, 2007, **99**(4), 048001.

13 I. C. Carpen and J. F. Brady, *J. Fluid Mech.*, 2002, **472**, 201–210.

14 D. G. A. L. Aarts, R. P. A. Dullens and H. N. W. Lekkerkerker, *New J. Phys.*, 2005, **7**, 40.

15 J. Zhao, D. Vollmer, H.-J. Butt and G. K. Auernhammer, *J. Phys.: Condens. Matter*, 2008, **20**(40), 404212, (8pp).

16 A. van Blaaderen and P. Wiltzius, *Science*, 1995, **270**(5239), 1177–1179.

17 A. Malevanets and R. Kapral, *J. Chem. Phys.*, 1999, **110**(17), 8605–8613.

18 R. E. Duff, F. H. Harlow and C. W. Hirt, *Phys. Fluids*, 1962, **5**(4), 417–425.

19 P. Kurowski, C. Misbah and S. Tchourkine, *Europhys. Lett.*, 1995, **29**(4), 309–314.

20 A. J. C. Ladd, *J. Chem. Phys.*, 1990, **93**(5), 3484–3494.

21 A. Lamura, G. Gompper, T. Ihle and D. M. Kroll, *Europhys. Lett.*, 2001, **56**(3), 319–325.

22 M. Ripoll, K. Mussawisade, R. G. Winkler and G. Gompper, *Europhys. Lett.*, 2004, **68**(1), 106–112.

23 Y. Inoue, Y. Chen and H. Ohashi, *J. Stat. Phys.*, 2002, **107**(1), 85–100.

24 C. P. Royall, R. van Roij and A. van Blaaderen, *J. Phys.: Condens. Matter*, 2005, **17**(15), 2315–2326.

25 K. O. Mikaelian, *Phys. Rev. E*, 1996, **54**(4), 3676–3680.

26 R. Biehl and T. Palberg, *Europhys. Lett.*, 2004, **66**(2), 291–295.